Petroleum Science 20 (2023) 1828–1842

Contents lists available at ScienceDirect

Petroleum Science

journal homepage: www.keaipublishing.com/en/journals/petroleum-science

Original Paper

Stress release mechanism of deep bottom hole rock by ultra-high-pressure water jet slotting

Hua-Jian Wang [a, b, c], Hua-Lin Liao [a, b, c, *], Jun Wei [a, b, c], Jian-Sheng Liu [a, b, c], Wen-Long Niu [a, b, c], Yong-Wang Liu [a, b, c], Zhi-Chuan Guan [a, b, c], Hedi Sellami [d], John-Paul Latham [e]

[a] School of Petroleum Engineering at China University of Petroleum East China, Qingdao, Shandong, 266580, China
[b] Key Laboratory of Unconventional Oil and Gas Development, Ministry of Education, Qingdao, Shandong, 266580, China
[c] Shandong Ultra-deep Drilling Process Control Tech R&D Center, Qingdao, Shandong, 266580, China
[d] MINES ParisTech, PSL-Research University, Geosciences Research Center, 60 bd Saint Michel, Paris, France VAREL Europe, 2 rue Johannes Kepler, 64000, Pau, France
[e] Earth Science and Engineering, Imperial College London, London, SW7 2AZ, United Kingdom

ARTICLE INFO

Article history:
Received 27 June 2022
Received in revised form
3 October 2022
Accepted 6 December 2022
Available online 7 December 2022

Edited by Jia-Jia Fei

Keywords:
Hard rock
Slotting
Stress release
Down hole pressures
Poroelastic mechanics
Fluid-structure Interaction
Ultra-high-pressure water jet

ABSTRACT

To solve the problems of rock strength increase caused by high *in-situ* stress, the stress release method with rock slot in the bottom hole by an ultra-high-pressure water jet is proposed. The stress conditions of bottom hole rock, before and after slotting are analyzed and the stress release mechanism of slotting is clarified. The results show that the stress release by slotting is due to the coupling of three factors: the relief of horizontal stress, the stress concentration zone distancing away from the cutting face, and the increase of pore pressure caused by rock mass expansion; The stress concentration increases the effective stress of rock along the radial distance from 0.6R to 1R (R is the radius of the well), and the presence of groove completely releases the stress, it also allows the stress concentration zone to be pushed away from the cutting face, while significantly lowering the value of stresses in the area the drilling bit acting, the maximum stress release efficiency can reach 80%. The effect of slotting characteristics on release efficiency is obvious when the groove location is near the borehole wall. With the increase of groove depth, the stress release efficiency is significantly increased, and the release range of effective stress is enlarged along the axial direction. Therefore, the stress release method and results of simulations in this paper have a guiding significance for best-improving rock-breaking efficiency and further understanding the technique.

1. Introduction

One of the factors affecting the performance of deep drilling operations is linked to the difficulty of breaking deep rock formations with an acceptable rate of penetration (ROP). Indeed, when they are subjected to strong geostatic stresses (due to the weight of the overlying rock masses and their tectonic deformation history over geological time) and hydrostatic pressures (due to the weight of the drilling mud column inside the well being drilled) (Chen et al., 2020, Hu et al., 2020a, 2020b, 2020c), the deep hard rocks become even stronger and less brittle when drilled by conventional drill bits (Fig. 1). This behavior, coupled with the abrasiveness and the natural heterogeneity of the rock matrix, drastically reduces the efficiency of the drilling process. This strengthening effect considerably increases the time required to carry out the last deep drilling sections and therefore the associated costs (Black and Judzis, 2004).

The distribution of the bottom-hole stress has been studied by some scholars (Zhang et al., 2018; Li et al., 2011), and the results show that bottom-hole stress can be divided into three types (triaxial tensile area, triaxial compressive area, tensile-compressive area). With the increase of depth, stresses are concentrated in the peripheral area of the bottom hole and reach several times the initial compressive *in-situ* values.

* Corresponding author. School of Petroleum Engineering at China University of Petroleum East China, Qingdao, Shandong, 266580, China.
E-mail address: liaohualin2003@126.com (H.-L. Liao).

https://doi.org/10.1016/j.petsci.2022.12.002

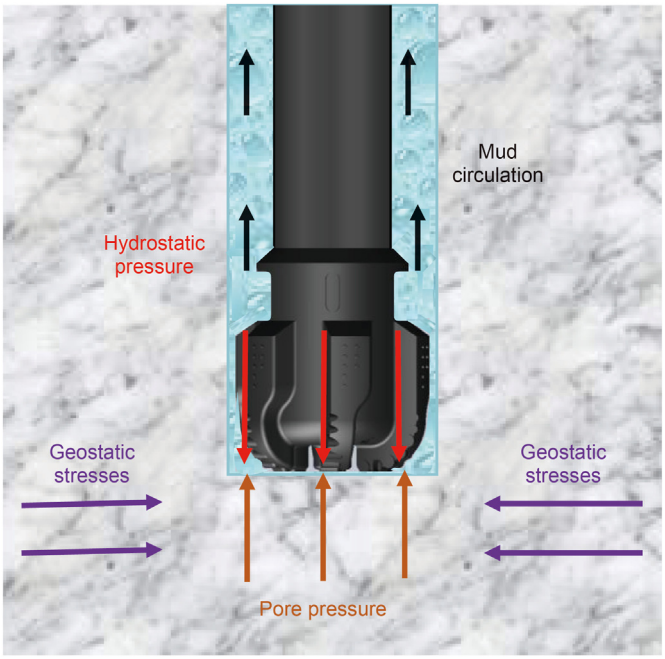

Fig. 1. Simplified representation of downhole pressures.

To solve the problems of high rock strength caused by high *in-situ* stress, it is mainly achieved by strengthening the outer bit tooth arrangement (Peng et al., 2006), optimizing the bit structure and tooth arrangement form (Hu et al., 2020a, 2020b, 2020c; Rhonda and Duey, 2017), and developing high-temperature and wear-resistant materials (Pan et al., 2016). In the aspect of improving the ROP, the new drill bit is mainly developed to change the stress state of the bottom hole. The maximum ROP of a self-adjusting dual-diameter PDC bit can be reached up to 70% higher compared to the conventional PDC bit (Gao et al., 2018; Durrand et al., 2010). The drilling rate of bionic abnormal shape hilarious diamond bit increases by 20%. At a certain drilling rate, its service life is more than twice the conventional PDC bit (Li et al., 2016). The reaming bottom hole and the collar hole wall of the steps have obvious rock stress release, good drillability, and help the PDC cutters to break the rock (Qin et al., 2019). Due to the weight of the drilling fluid column being decreased, underbalanced drilling alters the stress state compared with overbalanced drilling, the hydrostatic pressure being decreased, reducing the hold-down effect on cuttings of drilling fluid, promoting the bottom hole rock fragmentation and the migration of cuttings out of the bottom hole (Shi et al., 2018; Rumzan and Schmitt, 2001; Hui et al., 2012).

The auxiliary rock breaking tools mainly include positive displacement motor (Dong, 2010), turbo drilling technology (Xie et al., 2011), bit torsional impact generator (Xue et al., 2020; Shi et al., 2014), high-pressure jet drilling (Wang et al., 2012, 2022), vertical drilling tool (Ru et al., 2012; Wang et al., 2015) et al.. The high-pressure water jet assisting drilling was widely used in the field of well drilling engineering because of its good operability and high rock breaking efficiency (Liu et al., 2020; Liu et al., 2020; Liao et al., 2020), which can increase the drilling rate by 2–3 times (Huang et al., 2020; Liao et al., 2015; Huang and Wu, 2019). The water jet acts alone, producing a free surface, and the reflection of compressive stress wave on the free surface results in rock cracks, which improves the rock breaking efficiency (Wang, 2015); The pressurized fluid is ejected in the rock cracks and expands the cracks to cause rock fragmentation. Furthermore, the water jet can clean the cutter and wash away the rock fragments to prevent repeated crushing (Chen et al., 2020). In the aspect of the high-pressure jet assisting with teeth for rock breaking, the impact of teeth and jet respectively on rock results in the intersection and overlap of two groups of stress waves in rock, forming the expansion and intersection of cracks, which leads to the fragmentation of rock (Meng, 2019).

To sum up, the water jet can improve rock breaking ability by reducing the temperature and force of cutting tools, improving rock breaking ability, and prolonging the service life of cutting tools (Li et al., 2020). However, according to the interaction between the drill bit and water jet, it is found that the high-pressure water jet can also release the rock stress and reduce the rock strength. Therefore, the stress release method of rock slots in the bottom hole by ultra-high-pressure (UHP) water jet is proposed, and in this research, the stress release mechanism of rock is clarified. In addition, a fluid-structure coupling model was established to analyze the stress release effect of slotting. Finally, the rock strength function with confining pressure is fitted by the stress-strain characteristics of rock, and the effect of slotting on the rock strength is analyzed. This research proposes a method to speed up deep drilling and the stress release mechanism of bottom hole rock is clarified, which has a guiding significance for best-improving rock-breaking efficiency and understanding the technique still further.

2. Material and methods

2.1. Slotting method

The rock slotting method combines two previously separate, mature technologies: UHP water jetting and UHP Bit. In-hole production of the UHP water jetting using a down-hole pressure intensifier activated by the drilling vibrations or screw (Liu et al., 2017; Xie et al., 2011). The UHP Bit mainly consists of cemented carbide connectors, UHP channels, and UHP nozzles, which are arranged on the blades of the PDC bit, the high-pressure nozzle will rotate around the axis of the drill bit. The high-pressure fluid flow through the nozzle to break the rock, so the annular grooves will be generated at the bottom hole rock. Fig. 2 shows the slotting progress induced by water jet.

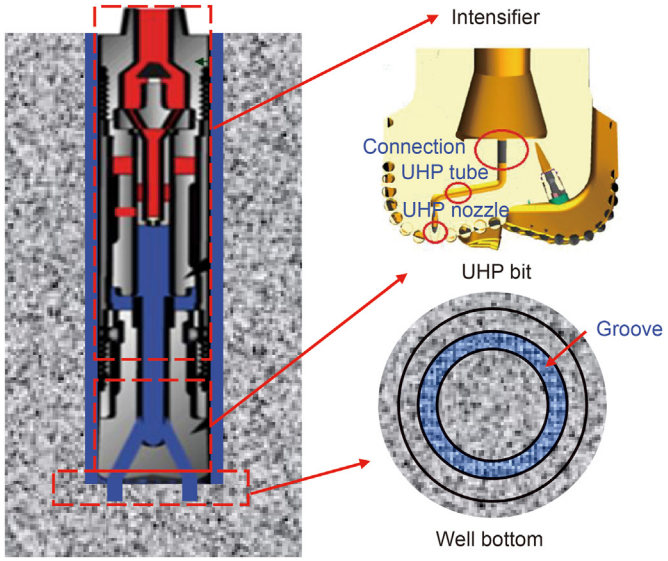

Fig. 2. Slotting progress induced by water jet.

When the UHP water jetting is produced by an intensifier, the rock will be broken, and with the PDC bit rotating, the circumferential single or multiple grooves will be generated, which depend on the number of UHP nozzles. The innovation lies in developing a new principle to 'free' the rock from these high confining stress concentrations in the local area of mechanical action of the cutters of the drilling bit, only a few millimeters below the bottom of the borehole. This will allow the mechanical drilling bit to break the greatly 'relaxed' and very weakened rock.

2.2. Stress release mechanism of slotting

The deepening of the drilling operation is always accompanied by a drastic drop in ROP due to the increase of geostatic stresses which, coupled with the hydrostatic pressure of the drilling fluid (mud), induces an increase in the strength and a reduction in brittleness of the rock. In the active area of the cutters of the drilling bit, these stresses will increase further because of the geometry of the hole, which induces a significant increase in rock resistance to the drilling action, causing a drop-in performance (Chen et al., 2020). Fig. 3 (where, p_p is pore pressure; σ_V is the overburden; σ_H and σ_h are maximum horizontal crustal stress and minimum horizontal crustal stress respectively) illustrates the distribution of the stresses at the bottom hole and shows that these stresses, increasing with depth, are concentrated in the peripheral area of the bottom of the well and reach several times the initial compressive *in-situ* values, which will be one of the main causes of the strength of the rock.

There are three functions of the circumferential groove. Firstly, the circumferential groove cuts off the connection between the wall and bottom, which interrupts the horizontal stress transmission, and the horizontal crustal stress is converted to the hydrostatic pressure of the drilling fluid. Because the hydrostatic pressure is smaller than the horizontal crustal stress, the stress of the bit-rock-mud interaction zone is reduced, Fig. 4 shows the downhole pressures regime with groove.

Secondly, the presence of the groove eliminates the phenomenon of sharp shape changes at the connection between the wall and bottom, and the stress concentrations in the local area of mechanical action of the cutters of the drilling bit disappeared. It also allows the stress concentration zone to be pushed away from the cutting face, while significantly lowering the value of stresses in the area the drilling bit acting.

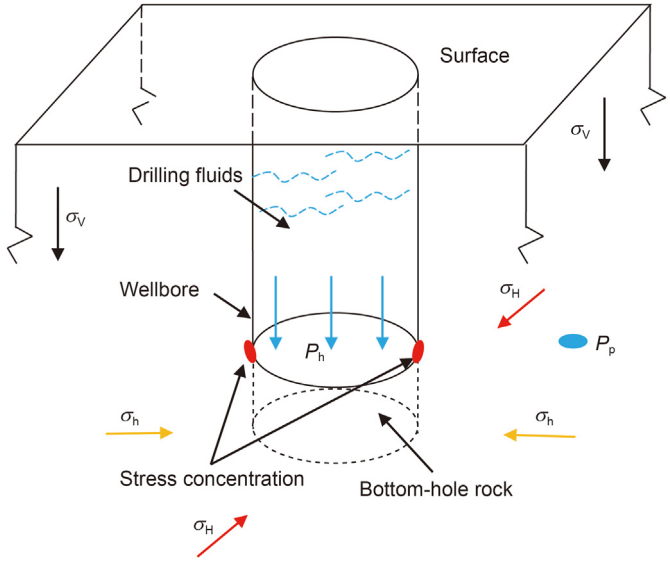

Fig. 3. Downhole pressures regime without groove.

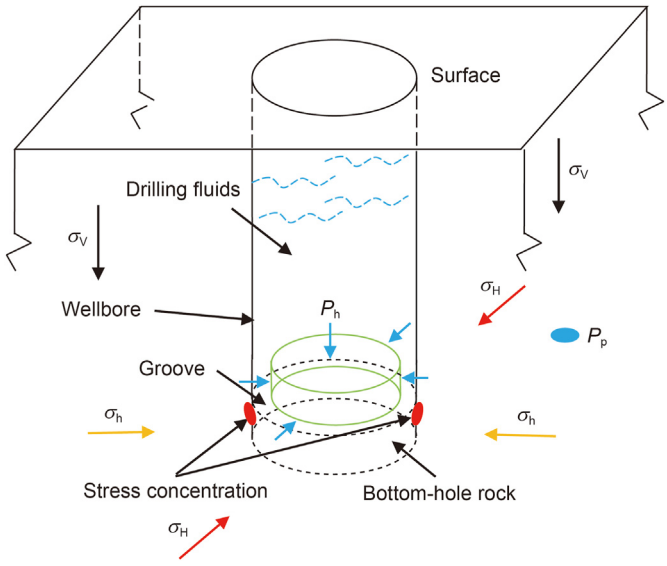

Fig. 4. Downhole pressures regime with groove.

Thirdly, because the presence of groove significantly lowers the value of stresses in the area the drilling bit acting, and causes the apparent density of the rock to decrease and expand, which results in further increases in the porosity and permeability of the bottom hole rock, the pressure is more smoothly transferred to the area the drilling bit acting.

$$a = \frac{\Delta e}{\Delta p} = \pm \frac{\rho_s}{\Delta p}\left(\frac{1}{\rho_m} - \frac{1}{\rho'_m}\right) \tag{1}$$

where, a is coefficient of compressibility, MPa^{-1}; e is void ratio, which is the ratio of the volume of voids in a solid to the volume of solid; p is effective *in-situ* stress, MPa; ρ_s is the density of solid particles in bottom hole rock, kg/m^3; ρ_m is the initial apparent density of bottom hole rock, kg/m^3; ρ'_m is the apparent density of bottom hole rock after effective stress changes, kg/m^3.

$$E_s = \frac{\Delta p}{\Delta \varepsilon} = \frac{1 + e_0}{a} \tag{2}$$

where, E_s is the modulus of compression, MPa; $\Delta\varepsilon$ is strain increment; e_0 is the initial void ratio of bottom hole rock (Sang et al., 2020).

2.3. Theory for the poroelasticity

2.3.1. Constitutive relations

As overburden is converted to hydrostatic pressure by drilling, the rock matrix will be deformed. To describe the interaction between pore fluid and rock matrix, the rock is regarded as poroelasticity material (Biot, 1962; Fjar et al., 2008; Liao et al., 2022):

$$\sigma = C : \varepsilon - \alpha_B p_p I \tag{3}$$

where, σ is Cauchy stress tensor; ε is strain tensor; α_B is Biot-Willis coefficient; p_p is pore pressure; C is the elasticity matrix; I is the unit matrix; ":" stands for the double-dot tensor product.

For isotropic linear elastic materials:

$$\mathrm{dev}(\sigma) = 2G_d \mathrm{dev}(\varepsilon) \tag{4}$$

where, G_d is the shear modulus.

The coupling of pore pressure and volumetric can be described by the following equation:

$$p_m = -k_d \varepsilon_{vol} + p_p \tag{5}$$

where, k_d is the bulk modulus of the porous matrix after drainage; ε_{vol} is the bulk strain, p_m is the average stress.

$$p_m = -\mathrm{trace}(\sigma)/3 \tag{6}$$

The change in pore pressure is as follows:

$$P_p = M(\zeta - \alpha_B \varepsilon_{vol}) \tag{7}$$

where, ζ is the fluid content; M is the Biot modulus, which is the reciprocal of the water storage coefficient S:

$$S = \frac{1}{M} = \left.\frac{\partial \zeta}{\partial P_p}\right|_{\varepsilon_{ii}} = \frac{\varepsilon_p}{K_f} + \frac{\alpha_B - \varepsilon_p}{K_s} \tag{8}$$

where, ε_p is porosity; K_f, K_s is the bulk modulus of the fluid and solid; α_B is Biot-Willis coefficient, which can be described by the following equation:

$$\alpha_B = \frac{\partial P_m}{\partial P_f} = 1 - \frac{K_d}{K_s} \tag{9}$$

2.3.2. Darcy's law

$$\nabla \cdot -\frac{k_m}{\mu}\left(\nabla p_p - \rho_l g\right) + \left(\frac{\alpha - \varphi}{k_a} + \frac{\varphi}{k_l}\right)\frac{\partial p_p}{\partial t} + \alpha \frac{\partial \vartheta}{\partial t} = q_m \tag{10}$$

where, k_m is the permeability of the rock skeleton; μ is the fluid viscosity, ρ_l is the fluid density, $\frac{\alpha-\varphi}{k_a}$ is the compression term of rock skeleton; $\frac{\varphi}{k_l}$ is the compression term of fluid; k_a, k_l is the bulk modulus of the rock skeleton and fluid respectively; φ is the porosity; $\alpha \frac{\partial \vartheta}{\partial t}$ is the volumetric strain term; q_m is the source sink term (Cheng, 2011).

2.3.3. Solid deformation

For a solid in an equilibrium state under the condition of gravity load, there is:

$$-\nabla \cdot \sigma = \rho_{av} \boldsymbol{g} = \left(\rho_f \varepsilon_p + \rho_d\right)\boldsymbol{g} \tag{11}$$

where, ρ_{av} is the densities of fluid and solid, ρ_f is the densities of fluid, ρ_d represent the densities of drained solid, respectively. The fluid-solid interaction is equivalent to input an additional volumetric term (as shown in Eq. (1)) into the stress tensor.

2.3.4. Cross-coupling term

Based on the results of Louis's experiment, cross coupling term between the above two equations is as follows (Louis, 1974; Wang et al., 2013),

$$k_f = k_0 e^{-\alpha' \sigma} \tag{12}$$

where, k_0 is the initial permeability coefficient; the effective normal stress is $\sigma = \gamma H - P$, γH is the weight of the overburden; this paper assumes that the principal direction of seepage and the principal direction of stress coincide, then the principal permeability coefficient is,

$$[k] = k_0 \begin{bmatrix} \exp(\lambda \sigma'_{e1}) & 0 & 0 \\ 0 & \exp(\lambda \sigma'_{e2}) & 0 \\ 0 & 0 & \exp(\lambda \sigma'_{e3}) \end{bmatrix} \tag{13}$$

where, λ is the influence coefficient; σ'_{ei} is the effective stress.

2.4. Numerical simulation method

2.4.1. Physical model

It is assumed that the pores are filled with fluid, while well inclination and temperature are ignored because of the obtained length of the well. And the influence of drilling fluid gradient is ignored. The pore pressure gradient is 0.0105 MPa/m. Overburden gradient is 0.024 MPa/m. Overburden gradient, maximum horizontal crustal stress gradient, and minimum-maximum horizontal crustal stress are adjacent to each other by 0.002 MPa/m. Table 1 shows the parameters of rock and drilling fluid.

The three-dimensional simulation model of down-hole rock is established, in which the length of the model is 2400 mm, the width is 2400 mm and the height is 2000 mm, the wellbore diameter is 240 mm and its depth is 1200 mm. In the vicinity of the wall and bottom hole, the mesh elements are finer than the remainder of the model. The simplified stress condition of deep rock is as shown in Fig. 5. The overburden is set at the top of the model, and the maximum horizontal crustal stress and minimum horizontal crustal stress are set at the surrounding of the model respectively. At the surrounding of the model and the bottom of the model is a set roller constraint. Hydrostatic pressure is set to the wellbore, and good permeability is assumed. The interaction between hydrostatic pressure and pore pressure is realized.

The simulation process is divided into two steps (Fig. 6), in the first step, *in-situ* stress balance is carried out, and the initial stress field is obtained using the Solid Mechanics Module. The stress field calculated in the first step is taken as the initial value of the Solid Mechanics Module in the second step, and then the stress field and seepage field of the stratum are solved in a modular fashion. The stress field and seepage field are coupled through a set of cross-coupling terms. The software COMSOL Multiphysics will convert the corresponding differential equations to the equivalent weak integral form and solve the algebraic equations according to the built-in algorithm to obtain the required stress or seepage field.

Table 1
Parameters of rock samples and drilling fluid.

Items	value
Modulus of elasticity, E, Gpa	60
Poisson's ratio, μ	0.25
Permeability coefficient, K, $m \cdot s^{-1}$	$1*10^{-7}$
Porosity, ε_p	0.1
The density of the rock sample, ρ_m, $kg \cdot m^{-3}$	2600
The bulk modulus of elasticity of rock, K_s, Mpa	60000
Pore fluid density, ρ_f, $kg \cdot m^{-3}$	1000
Fluid viscosity, μ_f, Pa•s	0.01
The bulk modulus of elasticity of fluid, K_f, Mpa	3270
Overburden, σ_V, Mpa	108
Maximum horizontal crustal stress, σ_H, Mpa	99
Minimum horizontal crustal stress, σ_h, Mpa	90
Pore pressure, p_p, Mpa	47.25
Liquid column pressure, p_h, Mpa	50.25

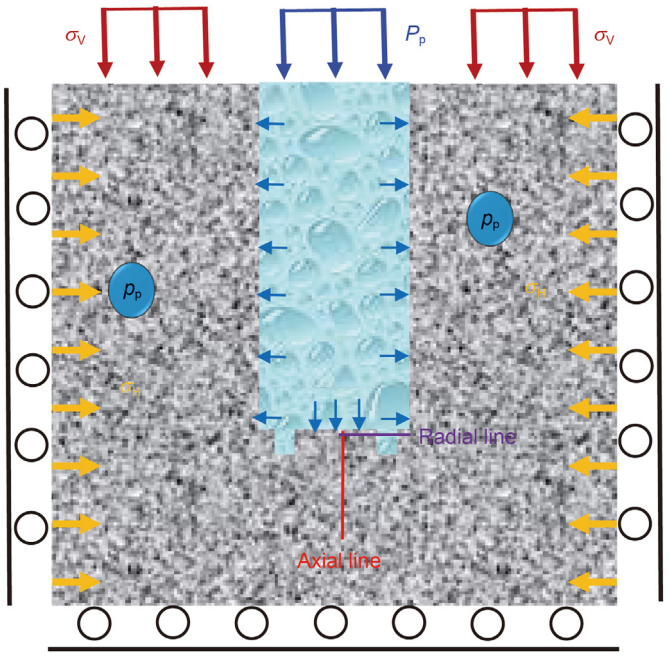

Fig. 5. Petrophysical model of the rock at bottom-hole.

2.4.2. Boundary conditions

To study the release efficiency of slotting with different groove structures, the numerical simulation parameters are shown in Table 2. It is vital to note that, in the process of slotting, the angle of water jet rotation represents the range of slotting; the depth of grooves is the distance between the area the drilling bit acting and the bottom of the groove; the groove width refers to the distance between the two ends of the groove; in the process of studying the effect of number of grooves, the grooves are set to be distributed evenly in radial direction. The length from the shaft wall is used to study the effect of groove location on release efficiency.

Table 2
Numerical simulation parameters.

Terms	values
Groove depth, mm	5, 10, 15, 20, 30, 40
Release evolution of slotting, °	40, 80, 120, 160, 180, 240, 280, 320, 360
Groove width, mm	2, 4, 6, 8, 10, 20
Number of grooves	1, 2, 3, 4, 5, 6
Groove Position, mm	0, 20, 40, 60, 80

The characteristic of grooves induced by ultra high-pressure water jet has been studied. When the jet pressure is 150 MPa, the groove depth can reach 15 mm, and the higher the pressure of the water jet, the longer the acting time, and the deeper the groove will be. It is also found that under certain conditions, water jet can generate a groove with a depth of 50 mm (Xu et al., 2021).

In terms of width, under the condition of a 0.5 mm nozzle diameter with a standoff distance of 10 times the nozzle diameter, the groove width can reach 5 mm. Furthermore, in the drilling process, the nozzle with a diameter of 2 mm will be used, and the groove is much wider. The annular groove position is representative of the installation position of the nozzle. The number of annular grooves represents the number of nozzles, so the simulation parameters are set as the contents in Table 2.

2.4.3. Model verification

With the interaction of maximum horizontal stress, minimum horizontal stress, overburden rock pressure, and pore pressure, the effective stress distribution around the linear elastic borehole is shown as the references (Hu et al., 2020a, 2020b, 2020c) and

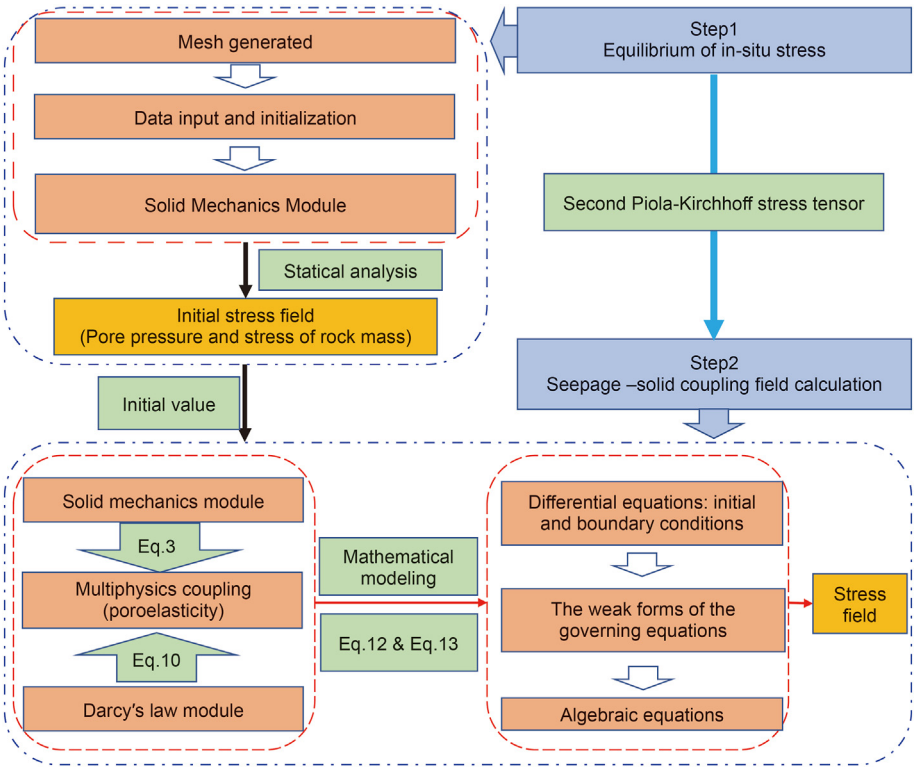

Fig. 6. Flow chart of numerical calculation.

(Charlez, 1997):

$$\sigma_r = \frac{(\sigma_H + \sigma_h)}{2}\left(1 - \frac{R^2}{r^2}\right) + \frac{(\sigma_H - \sigma_h)}{2}\left(1 + \frac{3R^4}{r^4} - \frac{4R^2}{r^2}\right)\cos 2\theta + \frac{R^2}{r^2}p_h - \alpha_B p_p \tag{14}$$

$$\sigma_\theta = \frac{(\sigma_H + \sigma_h)}{2}\left(1 + \frac{R^2}{r^2}\right) + \frac{(\sigma_H - \sigma_h)}{2}\left(1 + \frac{3R^4}{r^4}\right)\cos 2\theta - \frac{R^2}{r^2} - \alpha_B p_p \tag{15}$$

$$\sigma_z = \sigma_v - \mu\left[2(\sigma_H - \sigma_h)\left(\frac{R}{r}\right)^2 \cos 2\theta\right] - \alpha_B p_p \tag{16}$$

where, α_B is independent of fluid properties, but it depends on the properties of the porous matrix. For the softer porous matrix, the value of α_B is close to 1, whereas, the value of α_B for the harder matrix is close to the value of porosity. r is the radius in polar form, θ is the angle in polar coordinate; R is the borehole radius; μ is the Poisson's ratio.

Fig. 7 plots the stress around the borehole. The radial effective stress and hoop effective stress gradually approach the *in-situ* stress with the radial distance exceeding 5R, and the axial effective stress remains constant. The variation tendency of the numerical results and the analytical results are consistent, and the difference between the two is small, which indicates that the model is accurate, and that the simulation method has high reliability in analyzing the stress release characteristics.

3. Results and discussion

3.1. Pore pressure distribution

Fig. 8 compares pore pressure distributions before and after slotting. There is a pressure difference between hydrostatic pressure and pore pressure, and fluid displacement will occur between the drilling fluid and pore fluid. There is a pore pressure gradient in the rock, and the value of pore pressure near the borehole wall is equal to the hydrostatic pressure, but as the radial distance increases, the pore pressure in the rock gradually returns to the original pore pressure in the formation. Comparing the distribution of pore pressure before and after slotting, the presence of the groove increases the pore pressure and expands the influence range of drilling fluid pressure on pore pressure. According to the effective stress formula Eq. (17), increasing pore pressure can reduce the effective stress of rock (Hu et al., 2020a, 2020b, 2020c).

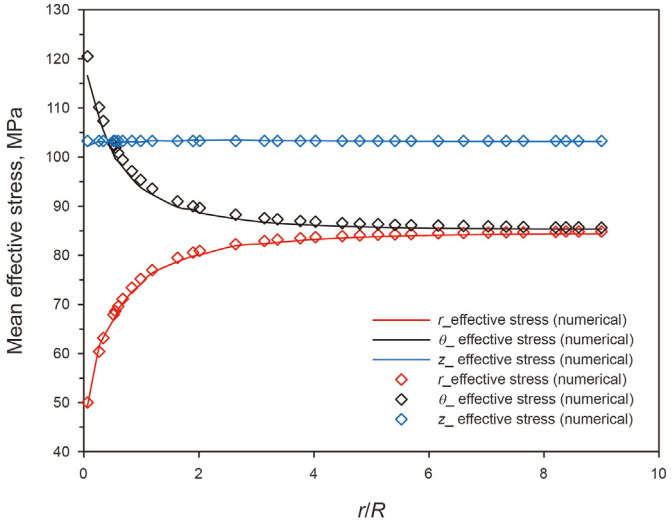

Fig. 7. Model verification.

$$\sigma_{eij} = 2G\varepsilon_{ij} + \lambda\vartheta\delta_{ij} - \alpha_B\delta_{ij}P_p \tag{17}$$

where, σ_{eij} is the effective stress, MPa; ε_{ij} is the strain tensor; λ is lame constant; ϑ is volumetric strain; δ_{ij} is the Kronecher function.

3.2. Dynamic evolution of effective stress during drilling

To study the dynamic evolution of effective stress during drilling, the single groove with a width of 2 mm and a depth of 20 mm is set at the junction between the borehole and the wall. Fig. 9 plots the dynamic evolution of bottom-hole stress during drilling. When the target point is 2.5R away from the bottom-hole at the borehole axis line, the effective radial stress is consistent with the *in-situ* stress, and the drilling does not affect the effective radial stress of the rock exceeding the range of 2.5R. As the depth increases with drilling, the radial effective stress at the borehole axial line present firstly increases and then decreases, the reason for this phenomenon is that, in the range of 0.9R–2.5R, the radial effective stress is affected by the stress concentration in the peripheral bottom-hole area, and with the increase of depth by drilling the distance between target point to the area of stress concentration is shortened. While, when the axial distance is less than 0.9R, as the depth increases further, the effective stress gradually decreases, which is due to the decrease of overburden pressure and the increase of pore pressure. Because of the stress concentration in the peripheral bottom-hole area, the rock at the target point of the borehole axis line will appear to be loaded firstly (the radial effective stress of the rock increases by 5%) and then unloaded (the radial effective stress of the rock decreases by 25%).

When the axial distance is exceeding 0.3R from the target point in the peripheral bottom-hole area (0.9R–1R). With the increase of axial distance, the radial effective stress gradually decreases from the original radial effective stress. While, when the axial distance is less than 0.3R, because of stress concentration, the radial effective stress of bottom hole rock sharply increases as the axial distance decreases, and the radial effective stress value is about 5 times the *in-situ* stress in the peripheral bottom-hole area. Therefore, the main reason for the increase in the stress of deep well bottom rock is not only the increase of *in-situ* stress and hydrostatic column pressure but also the stress concentrations local area of mechanical action of the cutters of the drilling bit.

Caused by drilling a sharp change of shape around the wellbore, thus the stress concentration around the bottom hole is generated, causing a sharp increase of stress, and stress will be diffused to the far field area in the form of stress bubble. The stress increases closer to the stress concentration area, and with the increase of distance, the stress diffusion will decrease, so the stress will be localized.

3.3. Effective stress distribution before and after slotting

Figs. 10 and 11 show the distribution of hoop effective stress and radial effective stress along the radial direction. When the deep rock is without a groove, the radial effective stress and the hoop effective stress increase with the increase of the axial distance. The reason for this phenomenon can be concluded that, as the axial distance increases, the stress release effect caused by the drilling

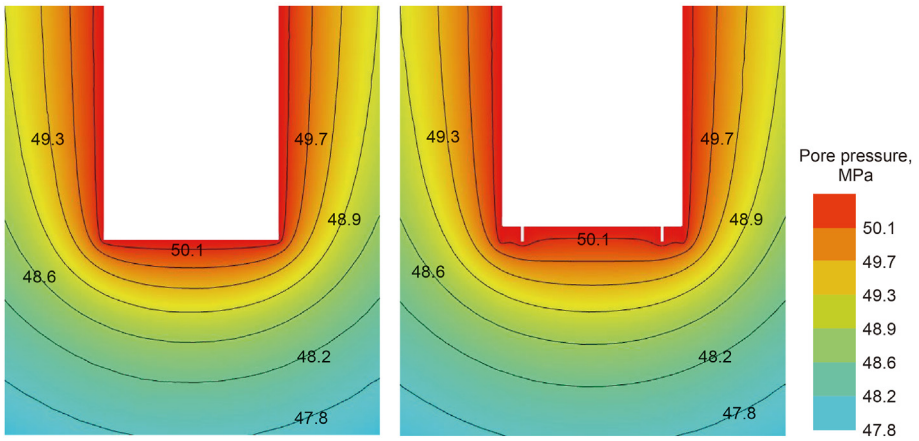

Fig. 8. Pore pressure distribution.

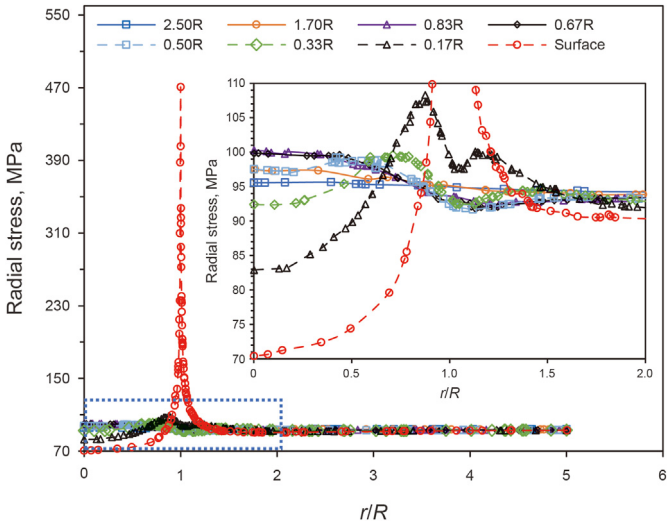

Fig. 9. Dynamic evolution of bottom-hole stress during drilling.

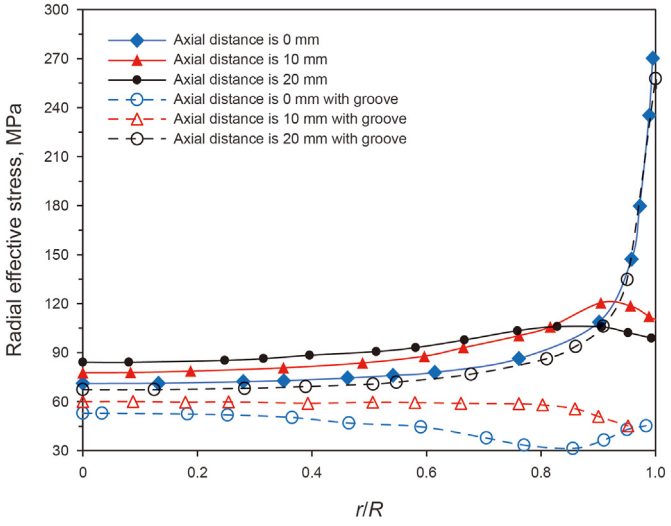

Fig. 11. Radial effective stress distribution.

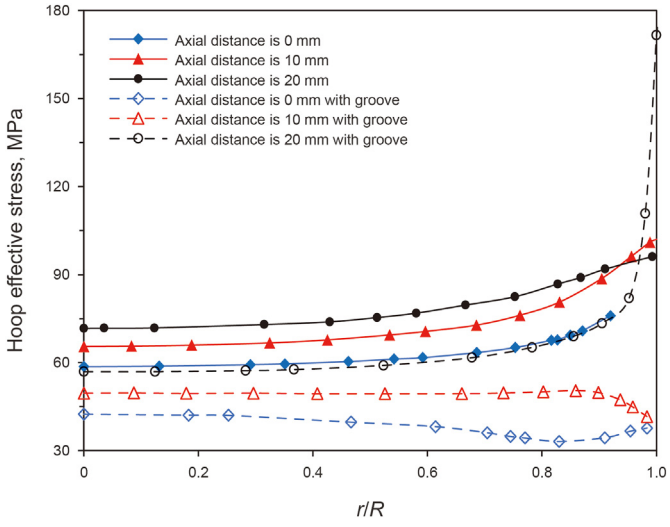

Fig. 10. Hoop effective stress distribution.

decreases. When the radial distance is in the range of 0–0.6R, with the increase of radial distance the effective stress is relatively stable, but exceeds 0.6R, with the increase of radial distance the effective stress increase, and the closer the area the drilling bit acting, the greater the effective stress is. In other words, the phenomenon of stress concentration will increase the effective stress of rock at the radial distancing 0.6R–1R.

After slotting, the radial effective stress and hoop effective stress both show a trend of increasing with the axial distance, and when the axial distance is 20 mm, the effective stress increase sharply. This is because the depth of the groove is 20 mm, and a new stress concentration phenomenon occurs in the bottom area of the groove. When the axial distance is 10 mm, the effective stress is relatively stable in the range of 0.85R. When it exceeds 0.85R, the effective stress begins to decrease. The reason for this phenomenon is that when the axial distance is 10 mm, the influence of stress concentration at the sharp corners of both ends is small, and the pore pressure increases significantly near the drilling fluid. When the axial distance is 0 mm, the effective stress is relatively stable in the range of 0–0.6R, while in the range of 0.6R–0.85R, it decreases,

and suddenly increases when it exceeds 0.85R. This is because after grooving, a new stress concentration will be generated in the area the drilling bit acting, resulting in the stress increase of the local area of mechanical action of the cutters on the drilling bit.

Comparing the distribution of effective stress before and after grooving, it can be found that the slotting can reduce the hoop effective stress and the radial effective stress, and the distribution characteristics of the two are similar, because there are only differences in values. Therefore, the stress release characteristics of radial effective stress are analyzed in this paper.

Fig. 12 shows the distribution of axial effective stress before and after the slotting. Within the scope of the study, in the range of 0–0.6R, the axial effective stress is not affected by the axial distance. But when the radial distance is exceeding 0.6R in the axial distance of 20 mm before the slotting, as the radial distance increases the axial effective stress shows a gradually increasing trend. The greater the axial distance, the more obvious the increase in the axial effective stress. The reason for this phenomenon is that the distribution of the effective stress decreases from the stress concentration area along the axial direction, while the range of influence is constantly expanding. After slotting, in the range of 0–0.9R, the axial effective stress of rock does not change with the axial distance increasing. But exceeding 0.9R, the axial effective stress decreases with the radial distance increasing. It is worth noting that the stress concentration occurs at the area with an axial distance of 20 mm due to slotting, which leads to a sharp increase in axial effective stress.

3.4. Effective stress release evolution during slotting

To study the stress release effectiveness (the definition of stress release efficiency refers to the ratio of stress after slotting to stress before slotting) of the bottom hole rock during slotting, the angle rotated by the UHP water jet represents the range of grooving, in which 0 represents the state without groove and 360° represents the complete formation of the circumferential groove in the bottom hole rock.

Fig. 13 compares the stress release efficiency with different angles at the borehole axial line. The radial effective stress release efficiency of rock is the highest in the area of the drilling bit acting, and the release efficiency decreases with the increase of the axial distance, and finally decreases to 0. It must be pointed out that the radial effective stress release range at the borehole axis line increases with the expansion of the slotting range.

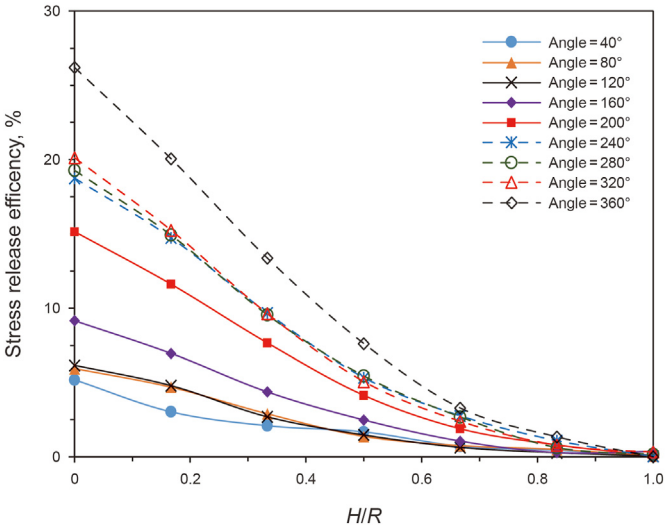

Fig. 13. Radial effective stress release efficiency at borehole axial line.

The radial effective stress release efficiency increases with the expansion of the slotting range. When the rotation angle of the jet is less than 200°, the radial effective stress release efficiency increases slowly. While the rotation angle is 200°, the release efficiency increases sharply. This is because the hydrostatic pressures replace the effect of horizontal crustal stress on bottom hole rock at both ends. As the slotting range further increases, the stress release efficiency shows a trend of slow growth again. After completely cutting off the connection of the wall and bottom hole, the stress on the bottom hole rock is completely converted from horizontal crustal stress to hydrostatic pressures, and the phenomenon of local stress rise caused by stress concentration is eliminated so that the stress release efficiency of bottom hole rock increases sharply.

Fig. 14 shows the axial effective stress release efficiency with different angles at the borehole axial line. In the range of 0–0.7R, the axial effective stress release efficiency shows a trend of sharply increasing with the increase of the axial distance. However, when the axial distance is greater than 0.7R, with the increase of the axial

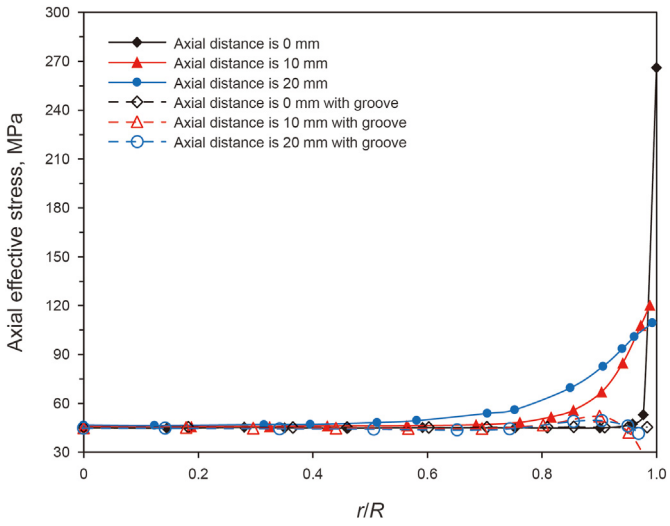

Fig. 12. Axial effective stress distribution.

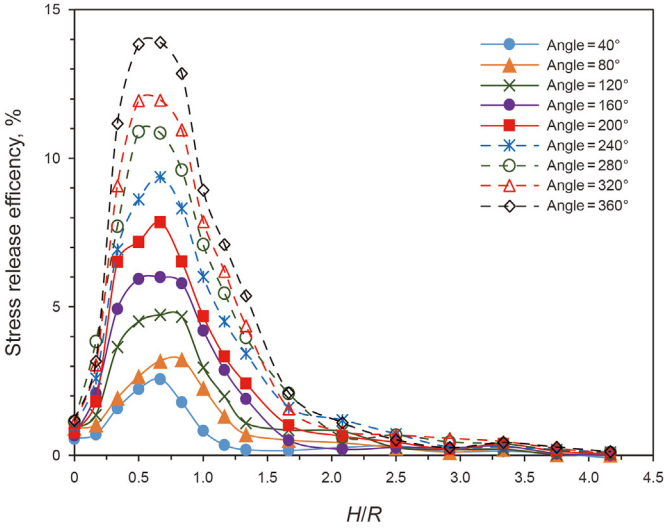

Fig. 14. Axial effective stress release efficiency at borehole axial line.

distance, the axial effective stress release efficiency decreases sharply at first and then slowly. The expansion of the slotting range significantly increases the release efficiency of axial effective stress and enlarges the stress release range of axial effective stress. The axial effective stress release efficiency is hardly affected by the range of groove in the area the drilling bit acting and shows a slight increase with the expansion of the slotting range.

Fig. 15 shows the radial effective stress release efficiency at a radial distance. When the slotting range is less than 200°, the stress release efficiency is small, and decreases with the increase of radial distance. While the slotting range increases to 200°, the bi-directional compression of horizontal crustal stress on bottom hole rock is eliminated, and the radial effective stress release efficiency increases sharply. The groove changes the shape of the bottom hole, and it also allows the stress concentration zone to be pushed away from the cutting face. Therefore, with the increase of radial distance, the radial effective stress release efficiency keeps increasing. At the beginning of slotting, the stress at the grooving position will first decrease, and the release range will also increase with the expansion of the groove range. Therefore, the radial effective stress release efficiency in the area the drilling bit acting presents a trend of increasing.

3.5. Effect of groove structure on stress release efficiency

3.5.1. Effect of groove depth on stress release efficiency

Fig. 16 shows the radial effective stress release efficiency at the borehole axial line. The radial effective stress release efficiency is the largest in the area of the drilling bit acting, the release efficiency decreases with the increase of axial distance. The stress range and stress release efficiency of rock at the borehole axis line increase with the increase of groove depth. The main reason for this phenomenon is that the groove 'free' the rock from high horizontal crustal stress in the local area of mechanical action of the cutters of the drilling bit, causing the apparent density of the bottom hole rock to decrease and expand. And this results in further increases in the porosity and permeability of the bottom hole rock, and the pressure is more smoothly transferred to the area the drilling bit acting.

Moreover, the area of the drilling bit is acting far away from the stress concentration area, which further decreases the effective stress of the bottom hole rock. The reason for this phenomenon can be explained by Saint Venant's Principle: if the plane stress on the boundary of a small part of a body is transformed into statically equivalent plane stress with a different distribution, then the stress component in the vicinity will change significantly, and the stress will decrease with distance, but the effect at distance is negligible. Therefore, the effective stress decreases as the area of the drilling bit acting is far away from the stress concentration area.

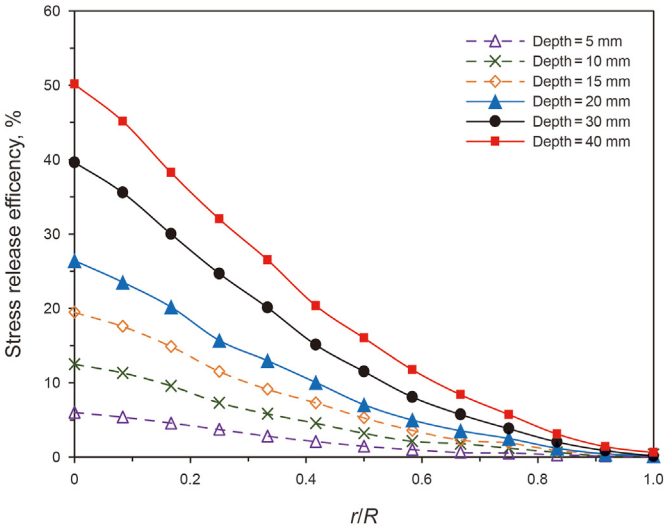

Fig. 16. Radial effective stress release efficiency at borehole axial line.

Fig. 17 shows the axial effective stress release efficiency at borehole axis line with groove depth. There is almost no release effect in the area the drilling bit acting with groove depth increasing. With the increase of axial distance, stress release efficiency firstly increases rapidly and then decreases slowly. With the increase of groove depth, the release efficiency of axial effective stress is significantly increased and the stress release range of axial effective stress is enlarged.

Fig. 18 shows the radial effective stress release efficiency alone the radial director with groove depth. When the groove depth is less than 15 mm, with the increase of radial distance the radial effective stress release efficiency increases slowly at first, and then increases sharply when it is close to the peripheral area of the

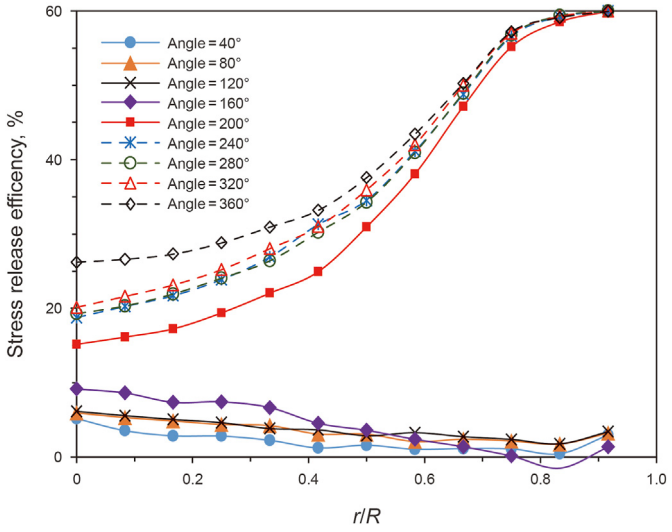

Fig. 15. Radial effective stress release efficiency at borehole radial line.

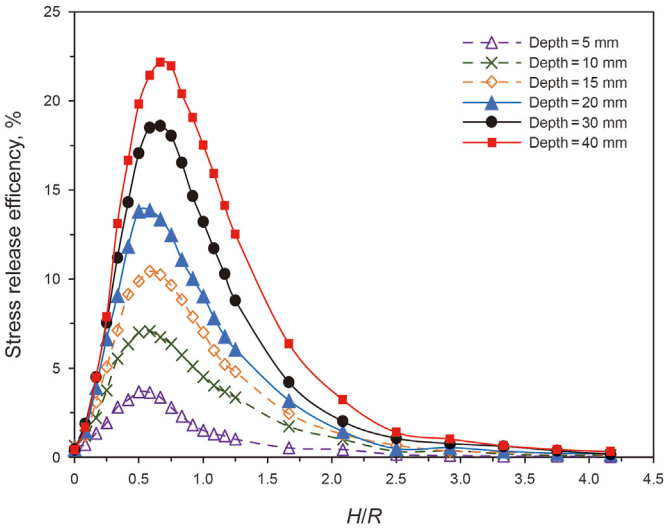

Fig. 17. Axial effective stress release efficiency at borehole axial line.

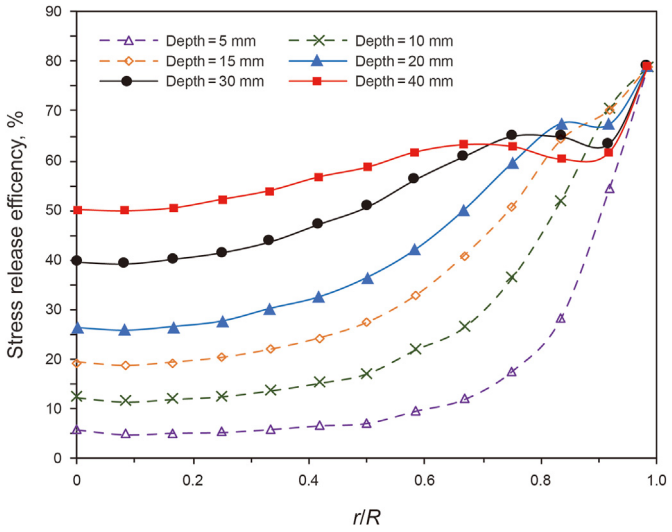

Fig. 18. Radial effective stress release efficiency at borehole radial line.

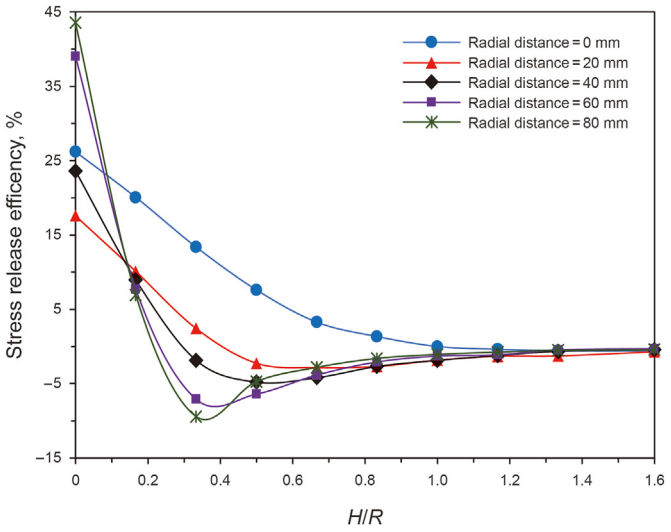

Fig. 19. Radial effective stress release efficiency at borehole axial line.

bottom-hole. When the groove depth is greater than 15 mm, with the increase of radial distance, the effective stress release efficiency first shows a slow increase, then gradually decreases, and finally increases rapidly.

Overall, groove depth has a great effect on stress release efficiency in the area the drilling bit acting. In the borehole axial line, the radial effective stress efficiency of rock in the area the drilling bit acting increases rapidly with the increase of groove depth. However, the release efficiency is less affected by grooving depth in the area peripheral area of the bottom-hole, and the stress release efficiency is about 80%. This is because with the increase of grooving depth, the effect of stress concentration on the peripheral area of the bottom-hole decreases, which reduces the stress in the area the drilling bit acting and increases the stress release efficiency. In addition, after slotting, the effective stress approaches to about 45 MPa, due to the action of drilling fluid, and the calculation formula is as follows:

$$\sigma = P_h - \alpha_B P_h \tag{18}$$

3.5.2. Effect of groove position on stress release efficiency

Fig. 19 compares the radial effective stress release efficiency with the grooving position, as the groove position moves towards the axis of the borehole, the stress release range decreases at the borehole axial line. The distance between the grooving position and the borehole wall is exceeding 40 mm, and the radial effective stress will be increased, the reason for this phenomenon can be concluded that the distance between the groove and the borehole axial line is closer, so the stress concentration caused by slotting increases the radial effective stress at the borehole axial line. The distance between the groove position and the borehole wall is 20 mm. The axial effective stress release efficiency of rock in the area the drilling bit acting at the shaft axis is the minimum, and the radial effective stress release efficiency of rock in the area the drilling bit acting will increase with the inward migration of the groove position.

Fig. 20 shows the axial effective stress release efficiency with the groove position. The stress release range and stress release efficiency of axial effective stress are the largest when the groove is in the borehole wall and decreases with the inward migration of the groove position at the borehole axial line.

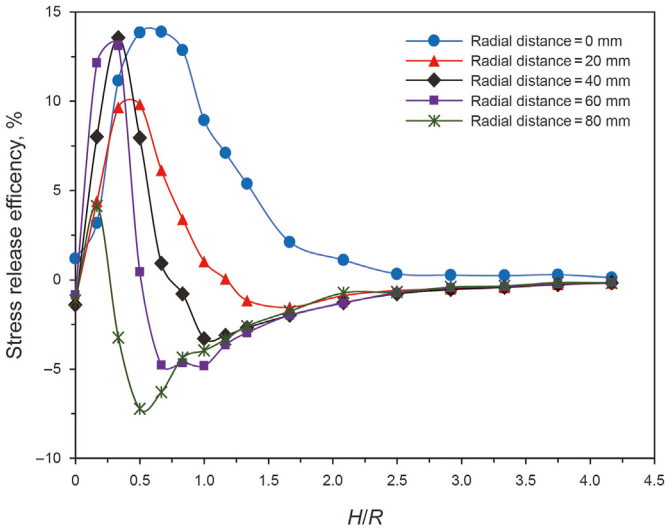

Fig. 20. Axial effective stress release efficiency at borehole axial line.

Fig. 21 shows the radial effective stress release efficiency along the radial direction. When the groove is located in the borehole wall, the radial effective stress release efficiency increases with the increase of radial distance. As groove position moving inward, the stress release efficiency increases in the inner region of the groove with the increase of radial distance, and reaches the maximum at the groove. While, with a further increase of the radial distance, the release efficiency decreases in the area the drilling bit acting. The closer the groove position is to the borehole axial line, the lower the release efficiency is, and even leads to increase of the stress concentration in the peripheral area of the bottom-hole. The reason for this phenomenon can be concluded that, when the groove is not located in the borehole wall, the stress concentration is still existing in the peripheral area of the bottom-hole, and the stress concentration gets more obvious as being closer to the borehole wall.

3.5.3. Effect of number of grooves on stress release efficiency

Fig. 22 shows the axial effective stress release efficiency with the number of grooves alone borehole axial line. In the axial range of 0–0.3R, the increase of the number of grooves can improve the

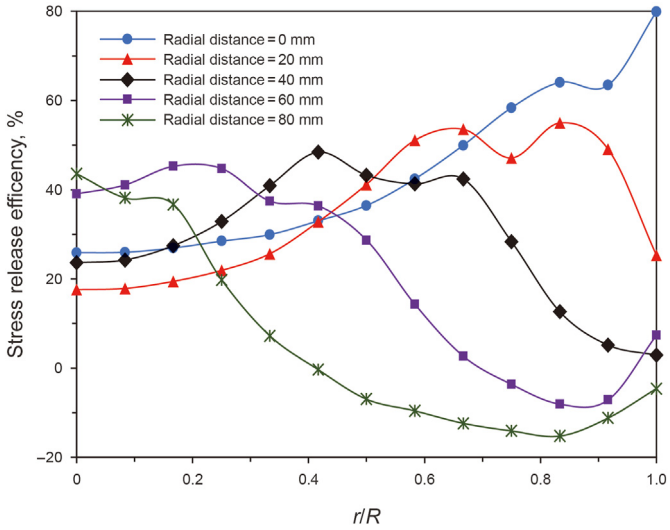

Fig. 21. Radial effective stress release efficiency at borehole radial line.

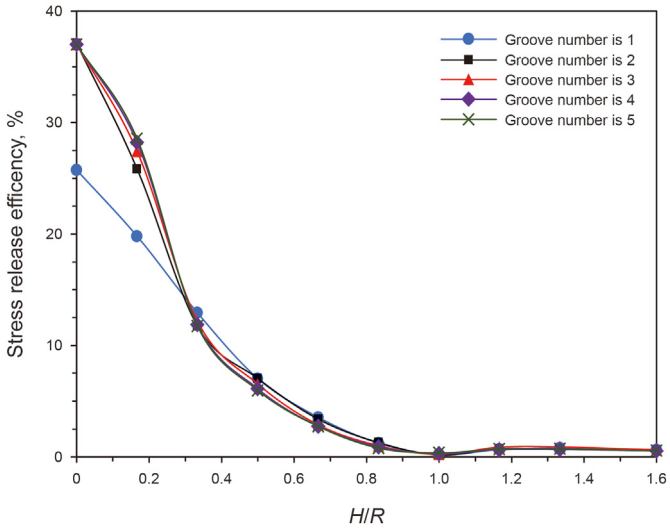

Fig. 22. Radial effective stress release efficiency at borehole axial line.

radial effective stress release efficiency. While the number of grooves is more than 2, the radial effective stress release efficiency along the borehole axis is hardly affected by the number of grooves, and the release efficiency decrease with the increase of axial distance. When the axial distance exceeds 0.3R, the release efficiency of grooves is not affected by the number of grooves, and the release efficiency goes to zero in where the axial distance is 1R.

Fig. 23 shows the radial effective stress release efficiency along the radial director in the area the drilling bit acting. The release efficiency increases first and then decreases with the number of grooves increasing. When the number of grooves is 1, the release efficiency is the lowest in the radial range of 0.6R. When the radial distance exceeds 0.6R and the number of grooves is 5, the stress release efficiency is the lowest. When the number of grooves is 3, the stress release efficiency is the highest. Although the increase in the number of grooves improves the effective stress release efficiency, it intensifies the fluctuation of the release efficiency curve and does not show a trend of continuous increase when there is a single groove. This is because the increase in the number of grooves will regenerate the stress concentration at the bottom of the

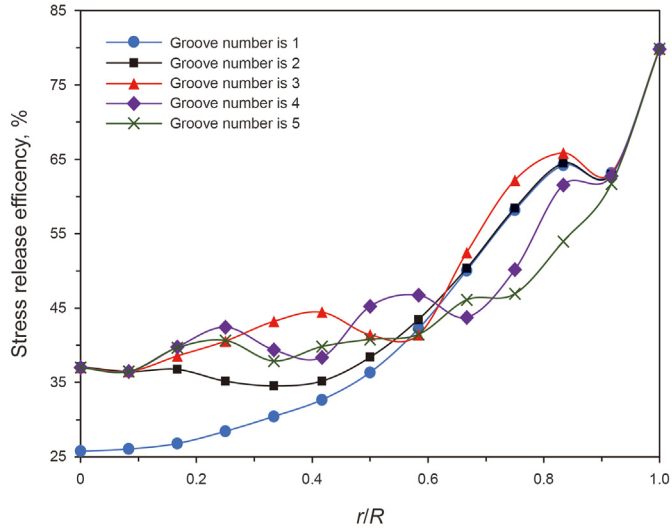

Fig. 23. Radial effective stress release efficiency at borehole radial line.

groove. Since the release efficiency of axial effective stress is hardly affected by the number of grooves, it is not discussed here.

3.5.4. Effect of groove width on stress release efficiency

To study the effect of groove width on release efficiency, the area where the drilling bit acting was selected to analyze the radial effective stress and hoop effective stress, and 0.8 mm away from the area where the drilling bit acting was selected to analyze the axial effective stress. Table 3 shows the effective stress release efficiency with groove width. It is not difficult to find out that the groove width has little influence on effective stress release efficiency. With the increase of groove width, effective stress release efficiency slightly increases. This is because the increase in the width of the groove reduces the distance between the drilling fluid and the borehole axial line, and the pore pressure increases at the borehole axial line, thus reducing the effective stress of the rock.

3.5.5. Effect of groove on compressive strength

Fig. 24 shows the comprehensive test system for high-temperature and high-pressure rock (Type: RTR-2000). The system uses an LVDT sensor to measure the strain of the specimen, its range is ±1.25 mm, the accuracy is 0.25%, the maximum test temperature is 200 °C, the maximum vertical working pressure is 2500 kN, the maximum horizontal principal stress can be applied is 80 MPa. The rock sample is Luhui granite with a cylinder size of 50 mm×100 mm. The experimental system and rock specimen are shown in Fig. 24.

The stress-strain relationship of the rock under confining pressures of 5, 10, 20, 30, 50 and 75 MPa was tested respectively, and the peak pressure was taken as the compressive strength of rock. The values of compressive strength and confining pressure of granite under different confining pressures were intercepted to make the scatter diagram as shown in Fig. 25.

Table 3
Effect of groove width on stress release efficiency.

Stress release efficiency, %	Groove width, mm						
	2	4	6	8	10	15	20
Radial	31.26	31.35	31.45	31.63	31.84	32.30	32.80
Hoop	30.86	30.98	31.00	31.12	31.17	31.41	31.72
Axial	13.43	13.82	14.69	14.74	15.53	16.45	16.95

Fig. 24. Rock mechanics experimental system.

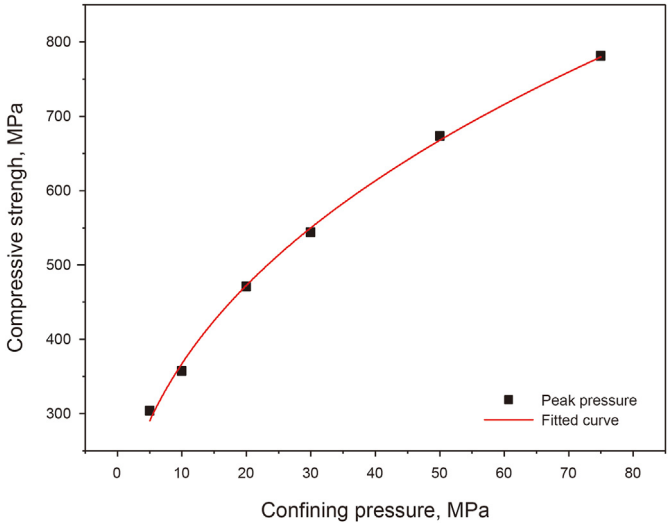

Fig. 25. The compressive strength with confining pressure.

The relationship between granite compressive strength and confining pressure was obtained by power function fitting, and the fitting degree was 0.9973. The fitting curve is as follows:

$$y = 144.35 \times (1 + x)^{0.389} \tag{19}$$

where, y is the compressive strength, MPa; x is the confining pressure, MPa.

In order to study the effect of slotting on rock compressive strength, the formula above are embedded into the software by the secondary development technology of numerical simulate software, and the relationship between strength and depth of grooves is analyzed by taking the depth of grooves as an example. Fig. 26 shows the compressive strength distribution, due to the effectiveness of horizontal crustal stress, hydrostatic pressures, and high confining stress concentrations in the local area of mechanical action of the cutters of the drilling bit, the compressive strength of rock is significant without a groove. When it starts to slot, the hydrostatic pressures replace the effect of horizontal crustal stress on the bottom hole rock at both ends. While, the effective stress increase caused by stress concentration still exists, so the release effect of strength is small. With the increasing of grooving depth, the distance between mechanical action of the cutters of the drilling bit and stress concentration area of groove increases, and the influence of stress concentration phenomenon on the rock in machine-rock action area decreases.

At the borehole axial line, the compressive strength is less than other areas without slotting, while, the compressive strength is higher than other areas after slotting. But, when the groove depth is exceeding 20 mm, the compressive strength at the area of the borehole axial line is the smallest in the mechanized rock action area. The reason for this phenomenon is that the groove depth is small, while the effectiveness of stress concentration is great, and the effectiveness of the stress concentration phenomenon in the machine-rock action area decreases with the increase of groove depth. In addition, with the increase of grooving depth, rock expansion increases in the mechanized rock action area, resulting in the apparent density of the bottom hole rock to decrease and expand and increase in the pore pressure, thus reducing the compressive strength of the rock in the mechanical action of the cutters of the drilling bit.

To illustrate the expanding characteristic of rock, Fig. 27 shows the volumetric strain with groove depth, the negative value represents the rock is compressed, and the volume decrease. The positive value represents the rock expansion. As can be seen from this picture, the phenomenon of rock expand are both appeared in the bottom hole and the borehole wall, and the bottom hole rock expansion is greater than the borehole wall, which is caused by overburden decreases in the action area of the drilling bit. As the increase of groove depth, the rock expansion becomes more obvious, and the expansion of rock stars from the slot position, and with the increase of the depth of the groove, the expansion range of rock gradually expands. This is because the increase of groove depth makes the stress concentration area away from the area the drilling bit acting, which reduces the compression effect of the stress concentration area on the rock. Due to the compression effect of stress concentration on rock, the volume of rock decreases rapidly in the area of stress concentration.

Rock expansion results in a decrease in the apparent density of bottom hole rock, which results in further increases in the porosity and permeability of the bottom hole rock, the pressure is more smoothly transferred to the area the drilling bit acting, causing the effective stress of the bottom hole rock is further reduced.

4. Conclusions

The stress release mechanism of rock is clarified: i. The annular groove cutting off the connection of wall and bottom, leading to interrupts the horizontal stresses transmission; ii. The groove allows the stress concentration zone to be pushed away from the cutting face, while significantly lowering the value of stresses in the area the drilling bit acting. iii. The value of stresses decreases, which causing the apparent density of the bottom hole rock to decrease and expand, and further increases in the pore pressure.

The main reason for the increase in the stress of deep well bottom rock are not only the increase of *in-situ* stress and hydrostatic pressure but also the stress concentrations local area of mechanical action of the cutters of the drilling bit (in the range of

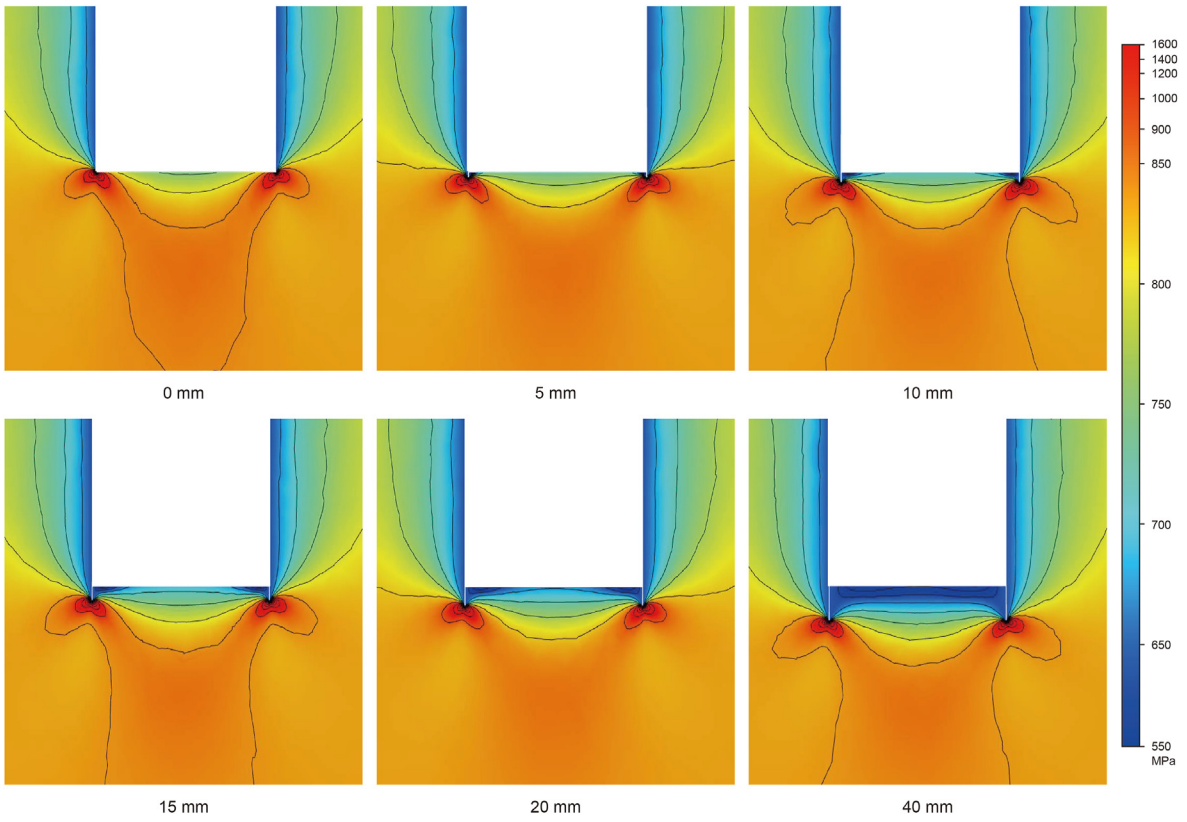

Fig. 26. Compressive strength distribution with groove depth.

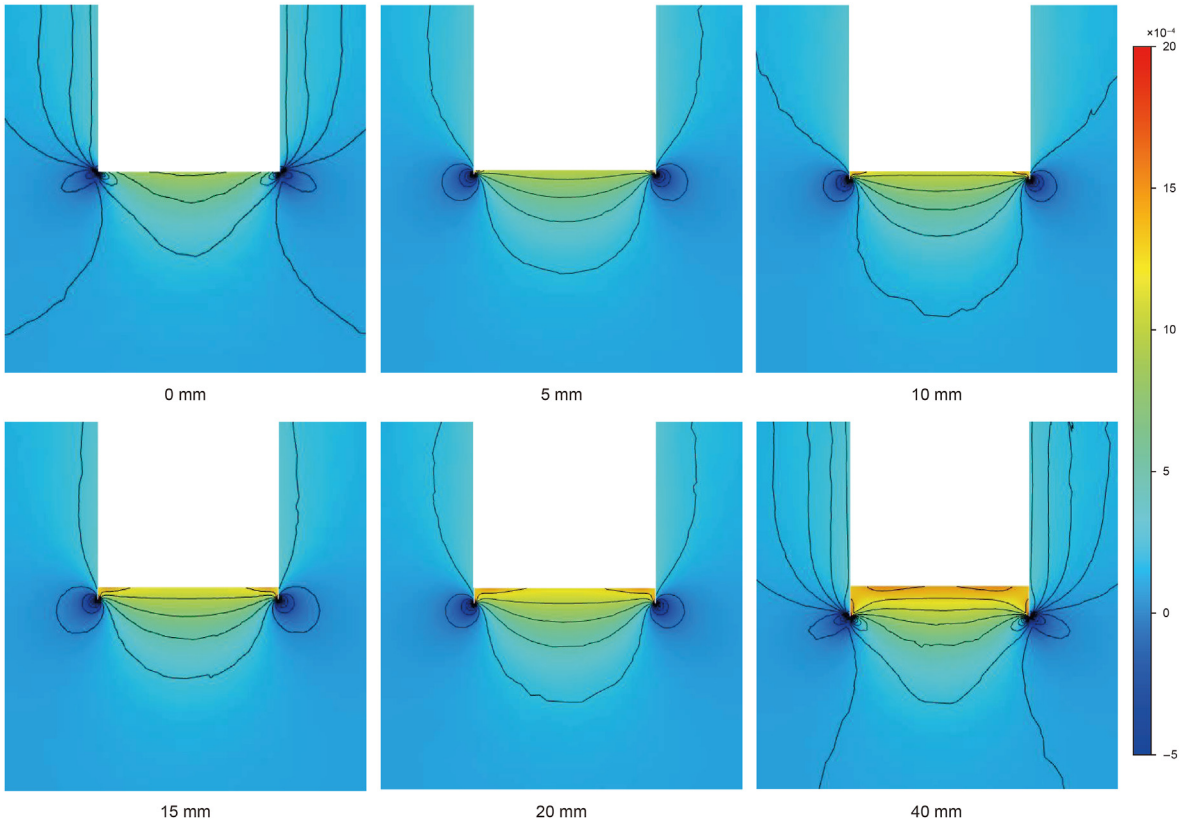

Fig. 27. Volumetric strain with groove depth.

0.6R ~ R along the radial distance). At the beginning of slotting, the stress at the grooving area will decrease, and the release range will also increase with the expansion of the groove range. After completely cutting off the connection of the wall and bottom hole the stress release efficiency increases sharply.

With the increase of groove depth, the release efficiency is significantly increased and the stress release range is enlarged. The stress release range and stress release efficiency are the largest when the groove is in the borehole wall and decrease with the inward migration of the grooving area at the borehole radial direction. Although the increase in the number of grooves improves the stress release efficiency, it intensifies the fluctuation of the release efficiency curve, the number of grooves is 3, the stress release efficiency is the highest. The release efficiency is hardly affected by groove width.

Calculating the compressive strength function, the strength condition of the rock at the bottom hole with different groove depths is analyzed. With the increase of grooving depth, rock expansion increases in the mechanized rock action area, resulting in the apparent density of the bottom hole rock decreasing and expand, and increase in the pore pressure, thus reducing the compressive strength of rock.

Acknowledgment

This paper acknowledges the support of the National Key Research and Development Program of China (2021YFE0111400), the Shandong provincial natural science foundation (No. ZR2019MEE120), and the horizon programme of the EU's funding of the ORCH YD project, EU-H2020 (101006752-ORCHYD).

References

Biot, M.A., 1962. Mechanics of deformation and acoustic propagation in porous media. J. Appl. Phys. 33, 1482–1498. https://doi.org/10.1063/1.1728759.

Black, A., Judzis, A., 2004. Optimization of deep drilling performance–development and benchmark testing of advanced diamond product drill bits & hp/ht fluids to significantly improve rates of penetration. Office of Scientific & Technical Information Technical Reports. https://doi.org/10.2172/836718.

Charlez, P.A., 1997. Rock Mechanics, vol. 2. Petroleum Applications, France. Web. https://www.amazon.com/Rock-Mechanics-Applications-Ph-Charlez/dp/2710805863.

Chen, P., Miska, S., Yu, M., et al., 2020. Poroelastic modeling of cutting bottom-hole rock – part i: stress state of bottom-hole rock - sciencedirect. J. Petrol. Sci. Eng. 189, 107014. https://doi.org/10.1016/j.petrol.2020.107014.

Chen, X., Cao, T., Yu, K., et al., 2020. Numerical and experimental investigation on the depressurization capacity of a new type of depressure-dominated jet mill bit. Petrol. Sci. 17, 1602–1615. https://doi.org/10.1007/s12182-020-00472-8.

Cheng, L., 2011. Advanced Seepage Mechanics. Petroleum Industry Press, Beijing.

Dong, M., 2010. Application of compound drilling technology in terrestrial formation in Yuanba Area. Petrol. Dril. Tech. 38, 38–40. https://doi.org/10.3969/j.issn.1001-0890.2010.04.010.

Durrand, C.J., Skeem, M.R., Hall, D.R., et al., 2010. Thick PDC, Shaped Cutters for Geothermal Drilling: A Fixed Cutter Solution for a Roller Cone Drilling Environment. American Rock Mechanics Association, USA, pp. 1–11. In: https://onepetro.org/ARMAUSRMS/proceedings/ARMA10/All-ARMA10/ARMA-10-524/118075.

Fjar, E., Holt, R.M., Raaen, A.M., et al., 2008. Petroleum Related Rock Mechanics. Elsevier, Trondheim. https://www.elsevier.com/books/petroleum-related-rock-mechanics/fjaer/978-0-12-822195-2.

Gao, K., Gao, H., Tan, X., et al., 2018. Application of bionic abnormal shape bit in dry rock drilling. J. Jilin Univ. (Earth Sci. Ed.) 48 (6), 1804–1809. https://doi.org/10.13278/j.cnki.jjuese.20170221.

Hu, H., Guan, Z., Shor, R., et al., 2020a. Dynamic response and strength failure analysis of bottom hole under balanced drilling condition. J. Petrol. Sci. Eng. 194, 107561. https://doi.org/10.1016/j.petrol.2020.107561.

Hu, H., Guan, Z., Xu, Y., et al., 2020b. Bottom-hole stress analysis of ultra-deep wells based on theory of poroelastic mechanics. J. China Univ. Petrol. (Edit. Nat. Sci.) 44 (5), 52–61. https://doi.org/10.3969/j.issn.1673-5005.2020.05.007.

Hu, H., Guan, Z., Zhang, B., et al., 2020c. Structure design of weight-on-bit self-adjusting PDC bit based on stress field analysis and experiment evaluation. J. Petrol. Sci. Eng. 196, 107692. https://doi.org/10.1016/j.petrol.2020.107692.

Huang, Z., Wu, X., et al., 2019. Mechanism of drilling rate improvement using high-pressure liquid nitrogen jet. Petrol. Explor. Dev. 46, 810–818. https://doi.org/10.1016/S1876-3804(19)60239-9.

Huang, Z., Zhang, S., Li, G., et al., 2020. Breakage mechanism of high-temperature granite by abrasive liquid nitrogen jet. Acta Pet. Sin. 41, 96–106. https://doi.org/10.7623/syxb202005009.

Hui, Z., Zhang, H., Guo, B., et al., 2012. Analytical and numerical modeling reveals the mechanism of rock failure in gas UBD. J. Nat. Gas Sci. Eng. 4, 29–34. https://doi.org/10.1016/j.jngse.2011.09.002.

Li, S., Dou, T., Dong, D., et al., 2011. Stress state of bottom-hole rocks in underbalanced drilling. Acta Pet. Sin. 32 (2), 329–335. https://doi.org/10.1007/s12182-011-0123-3.

Li, M., Su, Y., Sun, Y., et al., 2016. High matrix bionic abnormal shape impregnated diamond bit. J. Jilin Univ. (Eng. Technol. Ed.) 46, 1540–1545. https://doi.org/10.13229/j.cnki.jdxbgxb201605023.

Li, H., Liu, S., Jia, J., et al., 2020. Numerical simulation of rock-breaking under the impact load of self-excited oscillating pulsed waterjet. Tunn. Undergr. Space Technol. 96, 1–13. https://doi.org/10.1016/j.tust.2019.103179.

Liao, H., Guan, Z., Shi, Y., et al., 2015. Field tests and applicability of downhole pressurized jet assisted drilling techniques. Int. J. Rock Mech. Min. Sci. 75, 140–146. https://doi.org/10.1016/j.ijrmms.2015.01.014.

Liao, H., Jia, X., Niu, J., et al., 2020. Flow structure and rock-breaking feature of the self-rotating nozzle for radial jet drilling. Petrol. Sci. 17, 211–221. https://doi.org/10.1007/s12182-019-00378-0.

Liao, H., Wang, H., Niu, J., Wei, J., et al., 2022. Characteristics of stress release during downhole slotting by high-pressure water jet. Acta Pet. Sin. 43 (9), 1325–1333. https://doi.org/10.7623/syxb202209011.

Liu, Y., Guan, Z., Zhang, H., et al., 2017. Research status and prospect of ROP-enhancing technology based on drill string vibration. China Offshore Oil Gas 29, 131–137. https://doi.org/10.11935/j.issn.1673-1506.2017.04.017.

Liu, S., Zhou, F., Li, H., et al., 2020. Experimental investigation of hard rock breaking using a conical pick assisted by abrasive water jet. Rock Mech. Rock Eng. 53 (1), 4221–4230. https://doi.org/10.1007/s00603-020-02168-2.

Liu, Y., Cui, J., Wei, J., et al., 2020. Effect of nozzle structure on coal breakage of sc-co2 used for well drilling. Geomech. Geophys. Geo-Energy Geo-Resour. 6 (67), 1–21. https://10.1007/s40948-020-00199-1.

Louis, C., 1974. Rock Hydraulics in Rock Mechanics. Springer Verlag, New York, pp. 299–387. https://doi.org/10.1007/978-3-7091-4109-0_16.

Meng, D., 2019. Research on the Rock Breaking Performance of High-Pressure Pulsed Jet Assisted Mechanical Impact. China University of Mining & Technology. https://kns.cnki.net/KCMS/detail/detail.aspx?dbname=CMFD201902&filename=1019604468.nh.

Pan, J., Wang, M., Guang, X., et al., 2016. New progress and future development of PDC bit. China Petrol. Mach. 44, 5–13. https://doi.org/10.16082/j.cnki.issn.1001-4578.2016.11.002.

Peng, Y., Shen, Z., Fan, S., et al., 2006. Finite element model for analyzing stress field of bottom hole based on excavating method. Acta Pet. Sin. 27 (6), 133–136. https://doi.org/10.7623/syxb200606035.

Qin, L., Fu, W., Huang, Z., et al., 2019. Rock breaking characteristics of a single cone-PDC combined drill bit in hard formation. China Mech. Eng. 30, 2683–2690. https://doi.org/10.3969/j.issn.1004-132X.2019.22.006.

Rhonda, Duey, 2017. Smith bits, a schlumberger company: axeblade ridged diamond element bit. E & P: A Hart Energy Publ. 90 (5), 83–83. https://www.nstl.gov.cn/paper_detail.html?id=4d231f9f61e892ec3fde5cc00f72d829.

Ru, D., Zhang, J., Zhou, S., et al., 2012. Application of the vertical drilling system bh-vdt5000 on well keshen 203. Oil Dril. Prod. Technol. 34, 1–3. https://doi.org/10.13639/j.odpt.2012.04.004.

Rumzan, I., Schmitt, D., 2001. The Influence of Well Bore Fluid Pressure on Drilling Penetration Rates and Stress Dependent Strength. The 38th US Symposium on Rock Mechanics. American Rock Mechanics Association accessed. http://www.ualberta.ca/~dschmitt/papers/Rumzan_Schmitt_ROP_RockMech.pdf.

Shi, H., Li, G., Huang, Z., et al., 2014. Properties and testing of a hydraulic pulse jet and its application in offshore drilling. Petrol. Sci. 11, 401–407. https://doi.org/10.1007/s12182-014-0354-1.

Sang, S., Zhou, X., Liu, S., et al., 2020. Research advances in theory and technology of the stress release applied extraction of coalbed methane from tectonically deformed coals. J. China Coal 45 (7), 2531–2543. https://doi.org/10.13225/j.cnki.jccs.DZ20.0754.

Shi, H., Ji, Z., Zhao, H., et al., 2018. Investigations into the coiled tubing partial underbalanced drilling (CT-PUBD) technique for drilling hard formations. Petrol. Sci. 15, 830–840. https://doi.org/10.1007/s12182-018-0271-9.

Wang, H., 2015. Study on Rock Fragmentation Performance of High-Pressure Water-Jets Cutting Head and its Dynamics. China University of Mining & Technology. https://kns.cnki.net/KCMS/detail/detail.aspx?dbname=CDFDLAST2016&filename=1015972359.nh.

Wang, J., Zhang, J., Zhao, G., et al., 2012. Practice of 35 MPa high pressure jet drilling. Petrol. Dril. Tech. 40 (6), 22–26. https://doi.org/10.3969/j.issn.1001-0890.2012.06.005.

Wang, R., Shen, Z., Chen, X., et al., 2013. Full coupled analysis of seepage-stress fields for high arch dam based on COMSOL Multipysics. S2 Chin. J. Rock Mech. Eng. 32, 3197–3204. http://en.cnki.com.cn/Article_en/CJFDTOTAL-YSLX2013.

Wang, W., Wang, X., Yang, X., et al., 2015. Field test of full-rotation backup-type automatic vertical drilling tool. China Petrol. Mach. 43, 24–27. https://doi.org/10.16082/j.cnki.issn.1001-4578.2015.09.006.

Wang, H., Liao, H., Wei, J., et al., 2022. Pressure drop model and jet features of ultra high pressure water jet for downhole intensifier. ASME.J. Energy Resour. Technol. 144 (12), 123005. https://doi.org/10.1115/1.4054503.

Xie, L., Zhang, J., Zhang, D., et al., 2011. The application of turbo drilling technology

in yuanba key area. Petrol. Dril. Tech. 39, 15–18. https://doi.org/10.3969/j.issn.1001-0890.2011.06.004.
Xu, F., Zhou, H., Lu, J., et al., 2021. Research on combined rock-breaking mode of pre-cutting groove and TBM mechanical cutter, 2021 Rock Soil Mech. 42 (5), 1363–1372. https://doi.org/10.16285/j.rsm.2020.1468.
Xue, L., Han, H., Wang, D., et al., 2020. Experimental study on jet pulse assembly design and numerical simulation. Petrol. Sci. 17, 222–231. https://doi.org/10.1007/s12182-019-00396-y.
Zhang, R., Li, G., Tian, S., 2018. Stress distribution and its influencing factors of bottom-hole rock in underbalanced drilling. J. Cent. South Univ. 25 (7), 1766–1773. https://doi.org/10.1007/s11771-018-3867.